Biochemical Engineering Journal 106 (2016) 68–86

Contents lists available at ScienceDirect

Biochemical Engineering Journal

journal homepage: www.elsevier.com/locate/bej

# Modeling and simulation of continuous production of L (+) glutamic acid in a membrane-integrated bioreactor

Parimal Pal*, Ramesh Kumar, D. VikramaChakravarthi, Sankha Chakrabortty

*Environmental and Membrane Technology Laboratory, Department of Chemical Engineering, National Institute of Technology, Durgapur 713209, India*

ARTICLE INFO

*Article history:*
Received 10 May 2015
Received in revised form 25 October 2015
Accepted 10 November 2015
Available online 19 November 2015

*Keywords:*
Glutamic acid
Membrane bioreactor
Fermentation
Growth kinetics
Dynamic modelling
Scale-up

ABSTRACT

Modelling and simulation of direct and continuous production of L (+) glutamic acid under non-neutralizing conditions in a membrane-integrated bioreactor was done. The model describes a green and continuous process using sugarcane juice as a cheap and renewable carbon source for its microbial conversion to glutamic acid. Provisions of continuous withdrawal of product and downstream separation and recycle of microbial cells and unconverted carbon source allowed sustained production without pH adjustment. Appropriate microfiltration and nano-filtration membrane modules did the separation job efficiently. The model developed with extended Nernst-Planck approach captured the relevant transport phenomena along with fermentation kinetics under substrate-product inhibitions. Performance of the model is well reflected in low relative error (<0.05), high Willmott index ($d > 0.97$) and high overall correlation coefficient ($R^2 > 0.98$). The modelled system produced glutamic acid with a productivity of 8.2 g/(L h) and yield of 0.95 g/g at a reasonably high flux of 75 L/(m$^2$ h) under a transmembrane pressure of only 14–15 bar. The final product was obtained at a concentration of 55 g/L and could easily be concentrated further by an additional nanofiltration step.



## 1. Introduction

Amino acids like L-glutamic acid (GA) are widely used for human and animal nutrition, as ingredients of pharmaceutical products, cosmetics, agrochemicals and several other industrial derivatives. The demand for amino acids in the world market is in the magnitude of $10^6$ tons/year [1]. Conventionally amino acids have been produced by protein hydrolysis, microbiological fermentation, chemical synthesis, and enzymatic process. Efforts towards development of fermentative process for production of GA through isolation of L-glutamic acid-producing bacteria [2–4] have been quite significant in the recent years. Immobilization method of whole microbial cells has also been tried in calcium alginate or agar for continuous production of GA, but the product concentration remains low due to leakage of cells, inefficient mass transfer and lack of general matrix for immobilizing different cells [5]. Reported investigations of GA production mostly concentrate on using finished raw materials rather than a renewable or low cost waste material as carbon source [6]. In the back drop of prevailing low price of sugar cane in the major sugar cane growing countries (India, Brazil), large scale use of sugar cane juice as a clean, renewable carbon source for fermentative production of organic and amino acids holds the great promise of economic uplift of the millions of distressed sugarcane growers [7]. Efficient separation of other impurities from the fermentation broth is essential during downstream purification to produce monomer grade GA. Conventional purification schemes involve a number of downstream treatment steps like precipitation, filtration, acidification, neutralization, carbon adsorption and crystallization [2]. However conventional batch fermentation suffers from high labour cost due to frequent shutdown and start-up of batch process, low volumetric productivity and product-substrate inhibition. Moreover, such production processes are not eco-friendly and product purity and productivity are often compromised. Instead of direct production of acid, most of the investigated production schemes produce salt of the acid in pH-controlled regime necessitating further treatments with acids and alkalis to regenerate acid.

GA is produced through aerobic process of fermentation using *Corynebacterium* or *Brevibacterium* strains collectively known as *Corynebacterium glutamicum* [8]. Batch or fed-batch fermentation process is normally used for the commercial production of GA or

* Corresponding author. Fax: +91 343 254737.
*E-mail addresses:* parimalpal2000@yahoo.com, ppal.nitdgp@gmail.com (P. Pal).

http://dx.doi.org/10.1016/j.bej.2015.11.008
1369-703X/

**Nomenclatures**

*Microbial kinetics and continuous fermentation*

| | |
|---|---|
| $K_d$ | cell death rate constant ($h^{-1}$) |
| $K_{d,glu}$ | cell death rate constant while using glucose substrate ($h^{-1}$) |
| $K_{d,fru}$ | cell death rate constant while using fructose substrate ($h^{-1}$) |
| $K_{si,GA}$ | substrate inhibition constant for glutamic acid production (g/L) |
| $K_{si,s}$ | substrate inhibition constant for sugar consumption (g/L) |
| $K_{pi,GA}$ | product inhibition constant for glutamic acid production (g/L) |
| $K_{pi,s}$ | product inhibition constant for sugar consumption (g/L) |
| $K_{pi,X}$ | product inhibition constant for growth of biomass (g/L) |
| $K_{sl,GA}$ | substrate limitation constant for glutamic acid production (g/L) |
| $K_{sl,s}$ | substrate limitation constant for sugar consumption (g/L) |
| $K_{sl,X}$ | substrate limitation constant for growth of biomass (g/L) |
| $K_{glu,X}$ | glucose limitation constant for growth of biomass (g/L) |
| $K_{fru,X}$ | fructose limitation constant for growth of biomass (g/L) |
| $K_{si}$ | substrate inhibition constant (g/L) |
| $S_{glu}$, $S_{fru}$ | concentration of glucose and fructose (g/L) |
| $P$ | glutamic acid concentration (g/L) |
| $C_{bleed}$ | cell bleeding ratio |
| $V_f$ | working volume of the fermenter ($cm^3$) |
| $q_{GA,max}$ | maximum specific glutamic acid production rate (g/g h) |
| $q_{GA,net}$ | maximum specific glutamic acid production rate in continuous process (g/g h) |
| $q_{s,max}$ | maximum specific sugar utilization rate (g/g h) |
| $R^2$ | correlation coefficient |
| $S_0/S$ | concentration of the sugars (g/L) |
| $t$ | fermentation time (h) |
| $X$ | biomass concentration (g/L) |
| $X_{glu}/X_{fru}$ | biomass concentration generated when glucose or fructose used as substrate (g/L) |
| $X_t$ | biomass concentration in fermenter after starting of membrane cell recycles (g/L) |
| $S$ | substrate concentration (g/L) |
| $S_0$ | initial substrate concentration (g/L) |
| $S_{fer,ct}$ | substrate concentration in fermenter after continuous process (g/L) |
| $S_{rec}$ | substrate concentration in membrane cell recycle stream during continuous process (g/L) (negligible) |
| $P_{GA,fer,ct}$ | product concentration in fermenter after starting continuous process (g/L) |
| $P$ | product concentration in recycle stream of microfiltrate (g/L) |
| $Y_{XS}$ | biomass yield on sugar consumption |
| $Y_{SGA}$ | glutamic acid yield on sugar consumption |
| $J_{MF}$ | the solvent flux in permeate stream of microfiltration ($L/(m^2h)$) |
| $\Delta P$ | transmembrane pressure ($kg/cm^2$) |
| $R_m$ | membrane resistance ($m^{-1}$) |
| $R_f$ | membrane fouling resistance ($m^{-1}$) |
| $R_c$ | cake resistance ($m^{-1}$) |
| $J_s$ | uncharged solute flux (pore area basis) ($mol/m^2s$) |
| $J_v$ | volumetric flux of uncharged solute ($L/(m^2h)$) |

*Greek symbols*

| | |
|---|---|
| $\alpha$ | growth-associated constant in Luedeking–Piret model (g/g) |
| $\beta$ | net-specific growth rate ($h^{-1}$) |
| $\mu$, $\mu_{net}$ | specific growth rate ($h^{-1}$) |
| $\mu$ | maximum specific growth rate ($h^{-1}$) |
| $\mu_{glu}$ | specific growth rate for only glucose ($h^{-1}$) |
| $\mu_{fru}$ | specific growth rate for only fructose ($h^{-1}$) |
| $\mu_s$ | specific growth rate for only sucrose ($h^{-1}$) |

*Microfiltration and nanofiltration*

| | |
|---|---|
| $c_{w,i}$ | concentration of ion i ($mol/m^3$) on membrane wall |
| $c_{w,i,av}$ | average concentration of ion i ($mol/m^3$) on membrane wall |
| $C_{p,i}$ | concentration of ion i ($mol/m^3$) in permeate solution |
| $C_{B,GA}$ | bulk concentration of glutamate ($mol/m^3$) |
| $c$ | average concentration of uncharged solute concentration within pore ($mol/m^3$) |
| $D_{p,uc}$ | uncharged solute pore diffusion coefficient ($m^2/h$) |
| $D_i$ | hindered diffusivity of ion i ($m^2/s$) |
| $D_{b,i}$ | bulk diffusivity of ion i ($m^2/s$) |
| F | Faraday constant |

| | |
|---|---|
| $F_{in}$ | flow rate through which fermentation broth is coming in to fermenter ($cm^3/s$) |
| $F_{out}$ | flow rate through which fermentation broth is coming out from fermenter ($cm^3/s$) |
| $F_{rec}$ | flow rate through which cell has been recycled back to fermenter ($cm^3/s$) |
| $H$ | hindrance factor for convection of ion i |
| $H_{c,uc}$ | uncharged solute hindrance factor for convection |
| $J_{uc}$ | uncharged solute flux (pore area basis) ($mol/m^2s$) |
| $J_{GA}$ | solute flux of glutamate ion ($mol/m^2/s$) |
| $J_{MF}$ | the solvent flux in permeate stream of microfiltration ($L/(m^2h)$) |
| $k$ | Boltzmann constant, $1.38066 \times 10^{-23}$ J/K |
| $k$ | mass transfer coefficient of glutamate ion (m/s) |
| Pe | Peclet number (dimensionless) |
| $P_{GA,mf}$ | glutamic acid concentration (g/L) |
| $r_{mp}$ | effective pore radius (nm) |
| $r_{s,i}$ | solute radius of ion i (nm) |
| $R_{j,GA}$ | rejection of glutamic acid (%) |
| $R$ | universal gas constant (J/mol/K) |
| $R_m$ | membrane resistance ($m^{-1}$) |
| $R_f$ | membrane fouling resistance ($m^{-1}$) |
| $R_c$ | cake resistance ($m^{-1}$) |
| $T$ | absolute temperature (K) |
| t | fermentation time (h) |
| $V$ | radially averaged solution velocity (m/s) |
| $V_{pmv}$ | uncharged solute partial molar volume ($m^3/mol$) |
| $\Delta x$ | membrane thickness (m) |
| $X$ | biomass concentration (g/L) |
| $X_{Cm}$ | Electrical charged groups on the membrane surface ($mol/m^3$) |
| $z$ | valence of ion i |
| $\Delta P$ | effective pressure difference, ($kg/cm^2$) |
| $\eta$ | dynamic viscosity of the solution (kg/m/s) |
| $\Phi$ | steric coefficient |
| $\lambda_i$ | ratio of solute radius to pore radius of ion i |
| $\Delta\psi_s$ | Donnan potential difference (V) |
| $\Psi_E$ | electric potential |

monosodium glutamate. Production of glutamic acid by *C. glutamicum* is product-inhibited [9]. The existing models of kinetic behavior of biomass, substrate and product during GA production are mainly based on micro-kinetics- based mechanical approach or macroscopic-holistic approach [9–11]. Monod equation incorporated such product inhibition in the model of Levenspiel [12] which was subsequently used by Khan et al. [8]. However, most of such modeling studies have considered batch mode of production only.

In many studies, membranes have been used for separation of microbes from the fermentation broth. But in most of these cases, it has been a single stage membrane separation with microfiltration membrane in hollow fibre modules [13,14] and without any provision of recycling of unconverted carbon source and other media components. Thus a two stage membrane-integrated system has been considered in this study, to ensure cell- recycle and product recovery with continuous fermentation resulting in high cell density, higher productivity and yield. Emergence of tailor-made and novel membranes is gradually facilitating evolution of sustainable technologies for many chemical, biochemical and biotechnological production processes [15]. Modelling and simulation study along with economic analysis are necessary for raising scale-up confidence and ultimately transferring technology from laboratory to field. Kinetic modelling has been done in some of the cases but transport of GA through nano-filtration membrane has not received adequate attention. A few studies have been conducted on modelling of nanofiltration of amino acid through synthetic solution [16,17] but that too without considering the fermentation broth or bacterial kinetics.GA is an amphoteric electrolyte and its ionization state can be controlled by controlling pH of the feed solution which in turn plays significant role in mass transfer through the membrane. It is well established that an increase in the degree of ionization of amino acids results in increase in rejection capacity of the polymeric membranes [18,19].

Mathematical model based on multi-stage continuous GA fermentation system integrated with packed bed cell recycle scheme for high productivity was developed [20]. However, fouling prone hollow fibre membrane module was used in this model and the processing cost was high because of use of glucose as carbon source. The mathematical model for the nanofiltration system was developed following new linearized pattern by using experimentally determined model parameters such as concentration of electrically charged group on the membrane surface. The important model parameters such as the concentration of electrically charged group on the membrane surface ($X_{Cm}$) has been determined by conducting streaming potential experiments on each membrane unlike the previously reported approaches.

Models for continuous production of GA in fouling-free membrane-integrated system from a cheap and renewal carbon source capturing the both relevant kinetics and transport phenomenon especially during nanofiltration are practically absent in the literature. This modelling and simulation study along with economic evaluation is carried out to pave the industrial scale up of a new green design for production of GA.

## 2. Theory and model development

Dynamic mathematical transport model based on Extended Nernst-Planck (ENP) and Henderson-Hasselbalch equation has been developed here for the transport of both un-dissociated and dissociated forms of GA through nanofiltration. In the transport of neutral solutes (glucose, fructose, sucrose and un-dissociated glutamic acid), molecular diffusion and convection along with the steric phenomena play major role in nanofiltration membranes. In case of transport of charged solute (glutamate ion), Donnan exclusion principle governs separation [21,22].The fouling behaviour of nanofiltration membranes can be predicted by combining ENP equation with concentration polarization equation [23]. Analysis of microbial growth kinetics and production of GA have been done with the unstructured modelling approach of Luedeking-Piret. The standard assumptions of nanofiltration modelling, such as negligible viscosity gradient uniform membrane charge density and pore as cylindrical bundles within the membrane pores have been adopted.

### 2.1. Microbial kinetics equations during continuous fermentation

To identify growth kinetics of *C. glutamicum* (NCIM-2168) during fermentative production of GA from sugarcane juice, unstructured model was developed with Luedeking-Piret approach considering substrate limitation and substrate-product inhibitions. Monod model may be used for the substrate limitation whereas; substrate inhibition follows a non-competitive linear kinetic model (using Haldane equation). The substrate and product inhibition constant is captured in the model using the term '$K_i$' and '$K_{pi,GA}$'. The Eq. (1) shows the microbial growth rate during fermentation

$$\frac{dX}{dt} = (\mu_{net} - K_d)X \tag{1}$$

where, $\mu$ shows the specific growth rate and $K_d$ indicates biomass decay constant and $X$ is cell concentration in the fermenter. Considering the substrate inhibition and following the Haldane's approach the growth kinetics may be shown by Eq. (2),

$$\mu_s = \frac{\mu_{max} S}{K_s + S + (\frac{S^2}{K_i})} \tag{2}$$

where, $K_i$ represents the substrate inhibition constant and $K_s$ indicates the substrate limitation constant. Cell growth kinetics could be expressed in the presence of multiple substrates (viz. glucose, fructose), [24]:

$$\frac{dX}{dt} = (\mu_{max,glu}\frac{S_{glu}}{K_{glu,X} + S_{glu}} - K_{d,glu})X_{glu} + (\mu_{max,fru}\frac{S_{fru}}{K_{fru,X} + S_{fru}} - K_{d,fru})X_{fru} \tag{3}$$

Considering the conditions as shown in (Eqs. (1)–(3) and actual composition of substrate used in this study (i.e., carbohydrate composition in sugarcane juice), the growth rate of *C. glutamicum* (NCIM- 2168) could be derived as:

$$\frac{dX}{dt} = (\mu_{net} - K_d)X \tag{4}$$

where

$$\mu_{net} = (\mu_{glu}\frac{S}{S + K_{Sl,X} + (\frac{S^2}{K_i})} + \mu_{fru}\frac{S_{glu}}{K_{glu,X} + S_{glu}}\frac{S_{fru}}{K_{fru,X} + S_{fru}})(e^{-(\frac{P_{GA}}{K_{pi,X}})})$$

This Eq. (4) incorporates the term of the non-competitive product inhibition, which is essential for the determination of the specific growth rate of micro-organism [25]. In the fermentation broth the rate of substrate consumption may be expressed as:

$$\frac{dS}{dt} = q_{s,max}\frac{SK_{si}}{(K_{sl,s} + S)(K_{si,s} + S)}e^{-(\frac{P_{GA}}{K_{Pi,S}})}X \tag{5}$$

$K_{si,s}$ and $K_{sl,s}$ are substrate inhibition and limitation constants with respect to sugar consumption, and the maximum sugar utilization rate was denoted by $q_{S,max}$.

The modified form of Luedeking-Piret model could be used for expression of product formation in the fermentation broth as follows:

$$\frac{dP_{GA}}{dt} = \alpha\frac{dX}{dt} + \beta X \tag{6}$$

where α and β are growth and non-growth associated constants, respectively. Whereas, β may be expressed as,

$$\beta = q_{GA,max}\frac{SK_{si,GA}}{(K_{sl,GA} + S)(K_{si,GA} + S)}e^{-(\frac{P_{GA}}{K_{Pi,GA}})} \tag{7}$$

The overall equation for the product formation in the fermentation broth may be written as by combining Eqs. (6) and (7), as:

$$\frac{dP_{GA}}{dt} = \alpha\frac{dX}{dt} + q_{GA,max}\frac{SK_{si,GA}}{(K_{sl,GA} + S)(K_{si,GA} + S)}e^{-(\frac{P_{GA}}{K_{Pi,GA}})}X \tag{8}$$

The maximum specific GA production rate is denoted by $q_{GA,max}$ whereas $K_{si,GA}$, $K_{sl,s}$ indicate substrate inhibition and limitation constants during the product formation.

After 20 h of microbial growth, continuous operation starts at the exponential growth phase of the microorganism. The overall cell growth rate in the fermentation broth during steady-state considering the mass balance may be expressed as:

$$\frac{dX_t}{dt} = \left[\left(\frac{F_{rec}C_{bleed}}{V_f}\right) - \left(\frac{F_{out}}{V_f}\right) + \mu_{net}\right]X_t \tag{9}$$

$F_{out}$ represents the flow rate of the fermentation broth out of the fermenter and $F_{rec}$ represents the filtered fermentation broth recycle rate to the fermenter. The cell bleeding ratio is denoted by $C_{bleed}$ which plays a significant role in achieving the steady state condition [26]. The effective volume of the fermenter is represented by $V_f$.

Similarly, substrate consumption rate in the fermentation broth during continuous fermentation could be expressed considering the mass balance, substrate consumption, yield in terms of biomass and product formation with respect to substrate as [27]:

$$\frac{dS_{fer,ct}}{dt} = \left[\left(\frac{F_{in}}{V_f}S_0\right) - \left(\frac{F_{out}}{V_f}S_{fer,ct}\right) + \left(\frac{F_{rec}C_B}{V_f}S_{rec}\right) - \left(\frac{\mu_{net}}{Y_{XS}}X_t\right) - \left(\frac{q_{GAnet}}{Y_{PS}}X_t\right)\right] \quad (10)$$

Due to continuous removal of the product in the continuous fermentation process, the rate of substrate consumption is not subject to non-competitive inhibition. Here, $S_0$ indicates the substrate concentration in the fresh medium and $S_{fer,ct}$ is the substrate concentration at the end of the fermentation. The value of '$S_{rec}$' (substrate concentration in recycle stream) is almost negligible compared to $S_{fer,ct}$ and $S_{rec}$ because during cross flow microfiltration the residual substrate permeates through microfiltration membrane. $Y_{XS}$ and $Y_{PS}$ are the biomass yield and product yield on carbon source consumption respectively. Considering these conditions the product formation rate in the fermentation broth may be expressed as:

$$\frac{dP_{GA,fer,ct}}{dt} = \left[q_{GA,net}X_0e^{-(\mu_{net}t)} - \left(\frac{F_{out}}{V_f}P_{GA,fer,ct}\right)\right] \quad (11)$$

The maximum specific product formation rate is denoted by $q_{GA,net}$ in the continuous process and $P_{GA,fer,ct}$ is the product concentration (g/L) in the fermenter during continuous process. The term $X_t$ has been replaced by the $X_0e^{-(\mu_{net}t)}$as cell death has been considered negligible during continuous fermentation process. In addition to that $K_{pi,GA}$ is not consider in the above Eq. (11) as product inhibition is minimum as compared to the substrate inhibition $K_i$ due to continuous permeation of product through nanofiltration membrane.

### 2.2. Microfiltration

Mass transport through microfiltration membranes is largely dependent on the cake resistance at steady state condition [28]. The solvent flux through microfiltration may be calculated as:

$$J_m = \frac{\Delta P}{\mu_p\,(R_m + R_f + R_c)} \quad (12)$$

whereas $J_m$ represents the solvent flux in the permeate stream, $\Delta P$ is the transmembrane pressure, $R_{m,}$ is the membrane resistance, $R_f$ is the membrane fouling resistance occurs due to irreversible adsorption and pore plugging in membrane and $R_c$ is the cake resistance develops due to the formation of cake of biomass over the membrane surface.

### 2.3. Product purification by nanofiltration

The micro filtered fermentation broth contains uncharged solutes like sucrose and un-dissociated GA. In the final stage, nanofiltration is done for further downstream purification of micro filtered fermentation broth to get the pure form of GA which is governed by convection, diffusion and electrostatic charge repulsion mechanism [29].

Experiments were conducted in set flux method, in which the steady-state condition is ensured during continuous fermentation. In this approach, fine tuning in the rates of microfiltration and nanofiltration is done by exercising control on operating pressure, feed flow and recycle flow.

Under steady state condition, the changes in concentrations of product and substrate come to a halt and could be expressed as follows:

$$F_{nf,out}P_{GA,nf} = F_{nf,i}P_{GA,mf} - F_{nf,rec}P_{GA,nf,rec} \quad (13)$$

$$F_{nf,out}S_{s,nf} = F_{nf,i}S_{s,mf} - F_{nf,rec}S_{s,nf,rec} \quad (14)$$

where $F_{nf,i}$' and '$F_{nf,out}$' represents the input and output flow rates from nanofiltration membrane module. Similarly, $S_{s,mf}$ and $S_{s,nf}$ are the sugar concentrations at the input and output of nanofiltration membrane modules. The recycle flow rate from nanofiltration module is represented by $F_{nf,rec}$. $S_{s,nf,rec}$ and $P_{GA,nf,rec}$ are the carbon source and GA concentration in the recycle stream.

The fundamental transport equation to be used for uncharged solutes (GA) is the widely adopted modified hydrodynamic model which includes hindered convection and diffusion within the pores and it is expressed as [30]:

$$J_{uc} = VC_{p,uc} = (H_{c,uc}cV_{sol}) - \left(D_{p,uc}\right)\frac{dc_m}{dx} - \left(\frac{V_{pmv}cD_{p,uc}}{RT}\right)\frac{dP}{dx} \quad (15)$$

where hindrance factor for uncharged solute during convection is $H_{c,uc}$, $c_m$ is average concentration of uncharged solute concentration within pore and $D_{p,uc}$ is the coefficient of diffusion of product (GA) through membrane pores.

The solvent velocity ($V_{sol}$) can be computed by the help Hagen–Poiseuille relationships, which is expressed as:

(16) $V = \frac{r_{mp}{}^2\Delta P}{8\eta_{pw}\Delta X}$ where, $\Delta P$ is termed as effective pressure driving force and it is expressed as $\Delta P = (\Delta P - \Delta\pi)$. In that case, $\Delta\pi$ is termed as osmotic pressure difference between feed and permeate side and it can be computed by the following expression:

(17) $\Delta\pi = \left(C_{f,uc} - C_{p,uc}\right)$ RTwhere, $C_{f,uc}$ and $C_{p,uc}$ are the concentration of GA in the feed and permeate side respectively.

The concentration gradient of uncharged solute can be derived by Eq. (15) and it can be expressed as

$$\frac{dc}{dx} = \frac{Vc}{D_{p,uc}}\left[\left(H_{c,uc} - \frac{8\eta_{uc}D_{p,uc}V_{pmv}}{RTr_{mp}{}^2}\right) - \frac{C_{p,uc}}{c}\right] \quad (18)$$

Integration of the mass balance equation and performing algebraic manipulation after applying the suitable boundary conditions (BC 1: At $x = 0$, $c_m = \Phi_s \times C_{f,uc}$; BC 2: At $x = \Delta x$, $c_m = \Phi_s \times C_{p,uc}$) generates the equation:

$$C_{p,uc} = \frac{C_{f,uc}\left[H_{c,uc}\Phi_s - \left(\frac{8\eta_{uc}D_{p,uc}V\Phi_s}{RTr_{mp}^2}\right)\right]\exp\left(\frac{H_{c,uc}V_{pmv}RTr_{mp}^2\Delta x - 8\eta D_{p,uc}VV_{pmv}\Delta x}{D_{p,uc}RTr_{mp}^2}\right)}{\left[H_{c,uc}\Phi_s - \left(\frac{8\eta_{uc}D_{p,uc}V\Phi_s}{RTr_{mp}^2}\right)\right] - 1 + \exp\left(\frac{H_{c,uc}V_{pmv}RTr_{mp}^2\Delta x - 8\eta D_{p,uc}VV_{pmv}\Delta x}{D_{p,uc}RTr_{mp}^2}\right)} \tag{19}$$

From the definition of solute rejection, Rejection is expressed by

$$R_{j,uc} = 1 - \frac{C_{p,uc}}{C_{f,uc}} \tag{20}$$

To calculate the flux of anions like glutamate ions and to describe transport through nanofiltration membrane, the modified ENP equation may be used. Transport of negatively charged ions like glutamate ions through flat sheet cross-flow nanofiltration membranes may be expressed as the sum of the fluxes due to convection, diffusion and electro migration as follows:

$$J_{GA} = V \times C_{p,GA} = \left[(VH_{GA}c_{W,GA}) + \left(-D_{GA}\frac{dc_{w,GA}}{dx}\right) + \left(-\frac{Fz_{GA}c_{w,GA}D_{GA}}{RT}\frac{d\psi_s}{dx}\right)\right] \tag{21}$$

The pore inlet concentration of glutamate ions of membrane may be derived as follows:

$$\frac{dc_{W,GA}}{dx} = \left[\left(\frac{VH_{GA}c_{W,AC} - VC_{p,GA}}{D_{GA}}\right)\right] - \left[\left(\frac{Fz_{GA}c_{W,GA}}{RT}\right) \times \left(\frac{d\psi_s}{dx}\right)\right] \tag{22}$$

Similarly, the electro migration gradient $\left(\frac{d\psi_s}{dx}\right)$ through the membrane pores may be derived from Eqs. (21) and (22) :

$$\frac{F}{RT}\left(\frac{d\psi_s}{dx}\right) = \frac{\left[\left(\frac{H_{GA}V}{D_{GA}} - \frac{H_HV}{D_H}\right)c_{W,GA} - \left(\frac{V}{D_{GA}} - \frac{V}{D_H}\right)C_{p,GA} - \left(\frac{H_{GA}VX_{cm}}{D_H}\right)\right]}{(2c_{W,GA} - X_{Cm})} \tag{23}$$

The electro neutrality conditions within the pore and the permeate solutions are

$$z_{GA}c_{W,GA} + z_Hc_{W,H} = -X_{Cm} \tag{24}$$

$$z_{GA}C_{p,GA} = -z_HC_{p,H} \tag{25}$$

where $X_{Cm}$ is the electrical charged groups on the membrane surface and it can be computed by the following expression:

$$X_{Cm} = \frac{2}{r_{mp}F}\sqrt{\left(2\epsilon_V D_W K_B T \Sigma C_{f,i} N_A \left(\exp\left(-\frac{z_i e\xi}{K_B T}\right) - 1\right)\right)} \tag{26}$$

where,$\sigma_{mc}$,$\xi$,e, $D_w$, $K_B$,$\varepsilon_V$ and $N_A$ represents charge of the membrane, zeta potential of the membrane, electronic charge, dielectric constant of water, Boltzmann constant, vacuum permittivity and Avogadro's no respectively. $C_f$ and $T$ are concentration of the electrolytes and temperature at the time of investigation.

By substitutions of$c_{W,H}$,$C_{p,H}$ and $\frac{F}{RT}\left(\frac{d\psi_s}{dx}\right)$ into Eq. (22) yields below equation for finding the concentration gradient of negative ion:

$$\frac{dc_{W,GA}}{dx} = \left[\frac{\left\{\left(\frac{VH_H}{D_H} + \frac{VH_{GA}}{D_{GA}}\right)\left(c_{W,GA}^2 - X_{Cm}c_{W,GA}\right)\right\} - \left(\frac{c_{W,GA}C_{p,GA}V}{D_H}\right) - \left(\frac{C_{p,GA}V}{D_{GA}}\right)(c_{W,GA} - X_{Cm})}{(2c_{W,GA} - X_{Cm})}\right] \tag{27}$$

In the above equation, the numerator contain second order term whereas the denominator consists of first order terms only, so the concentration gradient $\left(\frac{dc_{W,GA}}{dx}\right)$ will be effectively constant throughout the membrane pore. Under these circumstances, the concentration profile can be estimated as follows:

$$\frac{\Delta c_{w,GA}}{\Delta x} = \left[\frac{\left\{\left(\frac{VH_H}{D_H} + \frac{VH_{GA}}{D_{GA}}\right)\left(c_{w,GA_{av}}^2 - X_{Cm}c_{w,GA_{av}}\right)\right\} - \left(\frac{c_{w,GA_{av}}C_{p,GA}V}{D_H}\right) - \left(\frac{C_{p,GA}V}{D_{GA}}\right)\left(c_{w,GA_{av}} - X_{Cm}\right)}{\left(2c_{w,GA_{av}} - X_{Cm}\right)}\right] \tag{28}$$

Using the principle of Donnan equilibrium, the concentration of charged ions are computed which is expressed by neglecting the salvation energy barrier as follows:

$$c_{w,i} = C_{B,i}\phi_i\exp\left(\frac{-z_iF\Delta\psi_s}{RT}\right) \tag{29}$$

By rearrangement of the above equation, the Donnan potential for the both positive and negative ions at the pore inlet is obtained by the following expression:

$$\Delta\psi_s(X = 0) = -\left[\left(\frac{RT}{F}\right)\ln\left(\frac{c_{w,H}}{\varphi_H C_{f,H}}\right)\right] = \left[\left(\frac{RT}{F}\right)\ln\left(\frac{c_{w,GA}}{\varphi_{GA}C_{f,GA}}\right)\right] \tag{30}$$

**Table 1**
Membranes characteristics used in this work according to manufacturer (Sepro Co., USA).

| Characteristics | Membrane | | | |
|---|---|---|---|---|
| | NF-1 | NF-2 | NF-3 | NF-20 |
| Membrane geometry | Flat-sheet | Flat-sheet | Flat-sheet | Flat-sheet |
| Membrane material | Polyamide | Polyamide | Polyamide | Polyamide |
| Membrane thickness (μm) | 165 | 165 | 165 | 165 |
| Solute rejection (%) at 10 bar pressure with solute concentration 2 g/L$MgSO_4$ (%) | 99 | 97 | 98 | 98 |
| NaCl (%) | 90 | 50 | 60 | 35 |
| Average molecular weight cut-off (Da) | 150–300 | 150–300 | 150–300 | 150–300 |
| pH Range | 3–10 | 3–10 | 3–10 | 3–10 |
| Maximum operating pressure (bar) | 83 | 83 | 83 | 83 |
| Maximum operating temperature (°C) | 50 | 50 | 50 | 50 |
| Membrane surface area used ($m^2$) | 0.01 | 0.01 | 0.01 | 0.01 |
| Deionized water permeability ($L/m^{-2}h/bar$) | 8–10 | 25–28 | 11–13 | 9–11 |
| Electrical charged group on the surface of NF membrane ($mol/m^3$)[a] | −1117 | −124 | −374 | −12 |

[a] Determined experimentally in present study.

$\Delta c_{w,GA}$and $c_{w,GA_{av}}$ may be computed by the help of Eq. (30) and these are expressed as:

$$\Delta c_{w,GA} = \frac{1}{2}\left[\sqrt{(X_{Cm}^2+4\varphi_H \times \varphi_{GA} \times C_{p,GA}^2)} - \sqrt{(X_{Cm}^2+4\varphi_H \times \varphi_{GA} \times C_{B,GA}^2)}\right] \quad (31)$$

$$\Delta c_{w,GA_{av}} = \frac{1}{4}\left[2X_{Cm} + \sqrt{(X_{Cm}^2+4\varphi_H \times \varphi_{GA} \times C_{B,GA}^2)} - \sqrt{(X_{Cm}^2+4\varphi_H \times \varphi_{GA} \times C_{p,GA}^2)}\right] \quad (32)$$

The following explicit expression for $C_{p,GA}$ can be obtained by rearrangement concentration gradient Eq. (28):

$$C_{p,GA} = \left[\frac{\left[(Pe_{GA}+Pe_H) \times \left(X_{Cm}c_{W,GA_{av}}\right)\right] - \left[(Pe_{GA}+Pe_H) \times c^2{}_{W,GA_{av}}\right] + \left[\left(2c_{W,GA_{av}} - X_{Cm}\right) \times \Delta c_{W,GA}\right]}{\left(\frac{Pe_{GA}X_{cm}}{H_{GA}}\right) - \left(\frac{Pe_H c_{W,GA_{av}}}{H_H} + \frac{Pe_{GA}c_{W,GA_{av}}}{H_{GA}}\right)}\right] \quad (33)$$

where, $Pe_{GA}$ and $Pe_H$ are the Peclet number of respective ions.

Rejection is calculated by the following expression

$$R_{j,GA} = \left(1 - \frac{C_{p,GA}}{C_{B,GA}}\right) \quad (34)$$

Similarly, volumetric flux can be computed by the following expression:

$$J_{vol} = \left(\frac{J_{GA}}{C_{p,GA}}\right) \quad (35)$$

The membrane wall concentration ($c_{w,GA}$) of the Glutamate ion can be measured by the 'concentration polarization' modulus which is depend on cross flow velocity on the membrane surface and the operation time. So the equation may be described as a function time and velocity:

$$c_{w,GA}(t,v) = \left[\left(1 - R_{j,GA}\right) C_{B,GA} + \left(C_{B,GA}R_{j,GA} \times e^{\left(\frac{J_{GA}}{k_m}\right)}\right)\right] \quad (36)$$

The detailed computation procedure of the model has been discussed in Section 3.6.

## 3. Materials and methods

### 3.1. Microbes, standards and membranes

*C. glutamicum* (NCIM 2168) is a Gram positive GA producing bacterium was bought from National Collection of Industrial Microorganism (NCIM), National Chemical Laboratory (Pune, India) in lyophilized condition. Standards of GA, sucrose, fructose and glucose were purchased from Sigma–Aldrich, USA. The microfiltration (MF) of fermentation broth was done by poly vinylidene fluoride (PVDF) hydrophilic MF membrane (Membrane solution, USA) having pore size 0.45 μm. Four different types of polyamide, flat-sheet NF membranes namely, NF-1, NF-2, NF-3 and NF-20 were purchased from Sepro Co. (USA). The detailed characteristics and properties of the membranes have been presented in Table 1.

### 3.2. Fermentation process

The pure sugarcane juice obtained from the local farmers was pre-filtered to remove suspended particles and used as fermentation media. The composition of seed culture medium was: urea, 5 g/L; yeast extract, 4; $K_2HPO_4$, 1 g/L; $MgSO_4{\cdot}H_2O$, 0.5; $FeSO_4{\cdot}7H_2O$, 0.02 g/L; biotin (5 μg/L); thiamine HCl (80 μg/L) and aqueous medium was sugarcane juice containing 11.0% (w/v) fermentable sugar. The heat sensitive chemicals like, urea, biotin and thiamine-HCl were cold sterilized by membrane filter (0.2 μm, PALL Life Sciences), whereas rest of the medium was sterilized separately by autoclaving at 15 psi (121 °C) for 15 min. The composition of production medium was same as the seed culture medium, but the urea and biotin concentration were 8 g/L and 1 μg/L respectively and tween 60 was added 0.1 mL/L of fermentation medium [8]. For glutamate fermentation by biotin-auxotroph *C. glutamicum*, biotin regulation is very important

for rapid growth of cells as well as GA production. The accumulation of GA is at maximum when the biotin concentration is suboptimal for maximum growth. The excretion of GA is also very important for its biosynthesis which in turn depends on the chemical and physical constituents of the cell membrane which is controlled by Tween 60 [31]. The pH of the production media, at the start and during the progress of fermentation was maintained 6.5–7.0 by sterile ammonia water (16.8%). The ammonia water serves dual function, as a pH-controlling agent and as nitrogen source, so it has great benefit over aqueous bases in maintaining the pH [31,32]. The temperature inside the fermenter was maintained 30 °C with water bath circulator (Polyscience, USA). Fermentation was started in the bioreactor of 30 L volume with 18 L fresh sterilized production media with 2 L (10%) seed culture of *C. glutamicum* (NCIM-2168), integrated with membrane separation system. pH and dissolved oxygen concentration (DO) were monitored using pH meter (ORION, 4 STAR, THERMO, USA) and DO meter (TOSHBRO, India). To maintain the desired DO concentration (5–7 mg/L), the sterile air was made to flow to the fermenter unit through spurge tube at the rate of 0.1 vvm with the help of a compressor and 0.22 mm disc filter (Millipore) in addition to provision of agitation at the rate of 250 rpm. The batch process continued up to 20–22 h and then continuous fermentation by adding fresh fermentation media with 0.1 $h^{-1}$ dilution rate and subsequent downstream purification began with continuous cell separation and recycle by cross-flow microfiltration membrane module attached to the fermenter. The microbial activity is maximised in the fermenter as substrate and product inhibitions are minimised through regulated flow of carbon source to the fermenter and continuous withdrawal of product. The provisions of continuous separation of cells and their recycle are resulting in fermentation under high microbial cell density. All these are eventually culminating in high conversion of carbon source as reflected in high yield and productivity of the membrane-integrated fermenter.

### 3.3. Analytical determination

Samples were ultra-centrifuged (Sigma Instruments, USA) at 10,000 × *g* and supernatants were collected for the analysis of GA, sucrose, fructose and glucose, whereas pellets were re-suspended with Milli-Q water for the measurement of cell growth by taking optical density ($OD_{660}$) through UV-VISIBLE spectrophotometer (Agilent Cary 60, USA). Concentration of carbohydrates and GA was measured using high performance liquid chromatography (Agilent, 1200 series, USA) with their respective columns. The measurement of glucose, fructose and sucrose was done with carbohydrate analysis column (Agilent Zorbax) at column temperature 30 °C with mobile phase acetonitrile: water (Milli-Q) (75:25 ratio) at flow rate 1.4 mL/min with sample injection volume 10 μL by refractive index detector (RID-G1362A). The retention time (RT) of fructose, glucose and sucrose were 4.08 min, 5.32 min and 8.12 min respectively. MCI GEL CRS 10W column (Mitsubishi Chemical Corporation, Japan) is used for the analysis of the GA with mobile phase 2 mM $CuSO_4$ at flow rate 1 mL/min at RT 16 min with Diode Array Detector (254 nm, DAD-G1315D). Flame Photometer (Labard, India) is used for the quantification of minerals like $Na^+$, $K^+$ and $Ca^{2+}$. Purity of the nanofiltered sample was determined by peak purity software tool of HPLC (Agilent 1200 series).

### 3.4. Experimental setup

Schematic diagram of the experimental setup has been shown in the Fig. 1. The experimental set-up was facilitated with thermostatically controlled vessel and instrumentations for monitoring flow, pH, temperature, dissolved oxygen and pressure. The experiments were investigated in two stages (MF and NF) flat-sheet cross-flow membrane modules with effective surface area of 0.01 $m^2$ for each membrane. The fermentation broth was made to pass through MF module by peristaltic pump (Entertech, India) followed by NF module by a high pressure (max. 40 bar) diaphragm pump (HYDRA-CELL, USA). The flow rate and operating pressure were controlled by a rotameter, a bypass valve and pressure indicator.

### 3.5. Determination of physico-chemical parameters

Regression analysis and curve fitting techniques were used for the determination of the physico-chemical parameters. To achieve the 'best fit' of the experimental data with the model predictions, least square approach was adopted. The model equations were solved in Microsoft Developer Studio-97 by using FORTRAN programming language.

### 3.6. Microbial growth associated constants

Microbial growth associated constants like product inhibition constant ($K_{pi,X}$) and the substrate limitation constant ($K_{sl,X}$) were computed by using modified Haldane equation Eq. (2) considering biomass cell concentration as the objective dependent variable and the substrate and product concentration as the independent variable in the EXCEL plot (EXCEL 2010). Glucose limitation constant ($K_{glu,X}$), fructose limitation constant ($K_{fru,X}$) and the substrate inhibition constant ($K_{si}$) have been computed by plotting the experimentally obtained results of growth of microbial mass against time. Substrate-inhibition constant for sugar consumption ($K_{si,s}$), product-inhibition constant for sugar consumption ($K_{pi,s}$), substrate limitation constant for sugar consumption ($q_{s,max}$) were calculated using Eq. (5) in the EXCEL plot. Here, substrate concentration is considered as objective dependent variable and the produced biomass concentration, as an independent variable. The substrate inhibition constant for GA production ($K_{si,GA}$), product inhibition constant for GA production ($K_{pi,GA}$), substrate limitation constant for GA production ($K_{sl,GA}$), the maximum specific GA production rate ($q_{GA,max}$) and the growth-associated constant in Luedeking–Piret model ($\alpha$) were the constant related to product formation and computed by using Eq. (6) following the same procedure.

### 3.7. Calculation of the membrane resistances during MF

Three different types of resistances like membrane resistance ($R_m$), cake resistance ($R_c$) and fouling resistance ($R_f$) are encountered during MF of fermentation broth. To calculate $R_m$ pure water flux ($J_w$) was computed experimentally through MF membrane, following relation is used:

$$R_m = \frac{\Delta P}{\mu \times J_w} \tag{37}$$

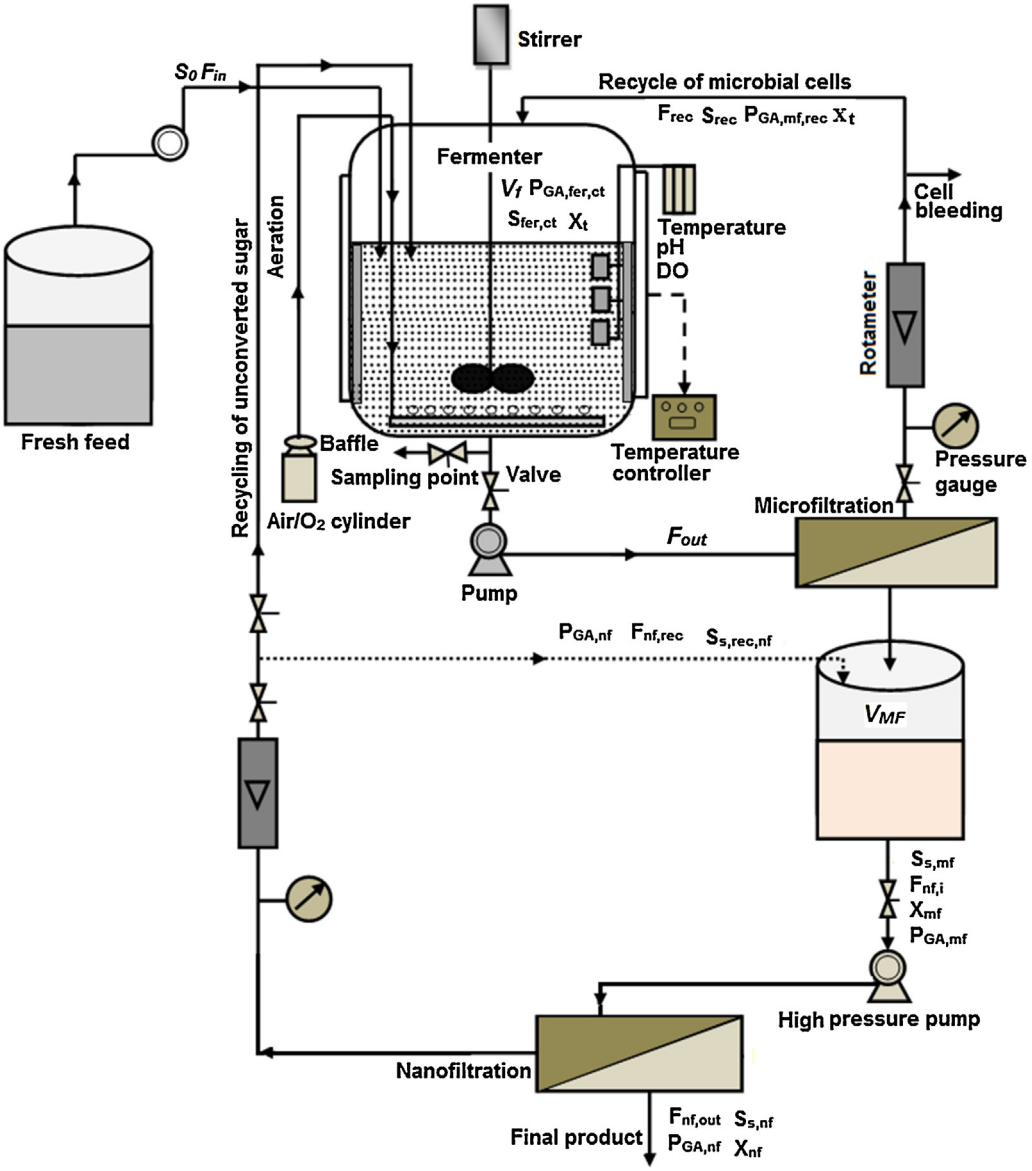


**Fig. 1.** Schematic diagram of membrane-integrated system used in investigation.

where $J_w$ represent pure water flux and $\mu$ represent the water viscosity. The following relation was used to compute the $R_c$:

$$R_c = \frac{m}{A}\alpha \Delta P^n \tag{38}$$

where $m$, $A$, $\alpha$ and $n$ indicate bacterial biomass, membrane surface area, cake resistant coefficient and compressibility index respectively [28]. $R_f$ value was calculated by subtracting $R_m$ value with $R_c$ value. PVDF membrane was used during the microfiltration of microbial cells present in fermentation broth. The membrane resistance ($R_m$) was evaluated $6.4 \times 10^{10}$ $m^{-1}$. In Eq. (38) the cake compressibility index ($n$) was calculated 0.58 depends on the particle size and its shape. The set flux method used during the microfiltration and constant permeate fluxes of 36 L/($m^2$h), 42 L/($m^2$h) and 49 L/($m^2$h) were maintained at three different cross-flow velocities of 0.53 m/s, 0.9 m/s and 1.25 m/s respectively at an operating pressure of 2.5 bar.

### 3.8. Computation of Peclet number

Peclet number may be computed by the following equation:

$$Pe_i = \left(\frac{H_i V \Delta x}{D_i}\right) \tag{39}$$

**Table 2**
Typical values of the used model parameters.

| Parameter | Symbol | Value | Unit |
|---|---|---|---|
| Pore radius of NF-1 membrane | $r_p$ | $0.53 \times 10^{-9}$ | m |
| Pore radius of NF-2 membrane | $r_p$ | $0.57 \times 10^{-9}$ | m |
| Pore radius of NF-3 membrane | $r_p$ | $0.55 \times 10^{-9}$ | m |
| Pore radius of NF-20 membrane | $r_p$ | $0.54 \times 10^{-9}$ | m |
| Solute radius of glutamate | $r_{s,GA}$ | $0.36 \times 10^{-9}$ | m |
| Solute radius of $H^+$ ion | $r_{s,H}$ | $0.025 \times 10^{-9}$ | m |
| Bulk diffusivity of glutamate | $D_{b,GA}$ | $0.74 \times 10^{-9}$ | $m^2/s$ |
| Bulk diffusivity of $H^+$ ion | $D_{b,H}$ | $9.4 \times 10^{-9}$ | $m^2/s$ |
| Bulk feed concentration | $C_f$ | 374 | $mol/m^3$ |
| Solution Viscosity | $\eta_s$ | 0.0015 | kg/ms |
| Electrolyte conductivity | $K_s$ | 2.2 | S/m |
| Vacuum permittivity | $\in_V$ | $8.854 \times 10^{-9}$ | C/V |
| Dielectric constant of water | $D_w$ | 78.5 at 25 | °C |
| Electronic charge | $e$ | $1.6022 \times 10^{-19}$ | C |
| Avogadro's no | $N_a$ | $6.022 \times 10^{23}$ | per mol |
| Temperature of operation | $T$ | 30 | °C |
| Boltzmann constant | $k$ | $1.38066 \times 10^{-25}$ | J/K |
| Faradays constant | $F$ | 96,500 | – |
| pKa value of glutamic acid (COOH-) | $pKa_{COOH^-}$ | 2.10 | – |
| pKa value of glutamic acid ($NH_3$) | $pKa_{NH3}$ | 9.47 | – |

### 3.9. Computation of hindered diffusivity ($D_i$)

Hindered diffusivity ($D_i$) may be computed by the multiplication of bulk diffusivity ($D_b$) and hindrance factor for diffusion ($H_d$) and expressed by the following relation:

$$D_i = D_{b,i} \times H_{d,i} \tag{40}$$

Hindrance factor for diffusion of ion i can be calculated by the following expression:

$$H_{d,i} = \left(1.0 - 2.3\lambda_i + 1.154\lambda_i^2 + 0.224\lambda_i^3\right) \tag{41}$$

$\lambda_i$ represents the ratio of solute radius to pore radius and it is expressed as:

$$\lambda_i = r_{i,s}/r_{mp} \tag{42}$$

### 3.10. Computation of Hindrance factor for convection of ion i ($H_i$)

It can be estimated by the following expression:

$$H_i = (2 - \phi_i)(1.0 + 0.054\lambda_i - 0.998\lambda_i^2 + o.44\lambda_i^3) \tag{43}$$

where,

$$\varphi_i = (1 - \lambda_i)^2 \tag{44}$$

### 3.11. Computation of zeta potential of the membrane

ξ is the Zeta potential of the membrane which can be computed by the following Helmholtz-Smoluchowksi equation:

$$\xi = \frac{\Delta S_p \eta_s K_c}{\Delta P \varepsilon_V D_W} \tag{45}$$

Here, $S_p$, $\eta_s$ and $K_c$ are the streaming potential, solution viscosity and electrolyte conductivity respectively. The concentration of electrically charged groups on the membrane surface of different nanofiltration membranes has been shown in a Table 1.

### 3.12. Computation of effective membrane thickness ($\Delta x$) and pore radius ($r_p$)

Computation of $\Delta x$ and $r_p$ was done during the validation of rejection and flux data by the model-predicted results with the experimental one while separating the uncharged solutes like sucrose. Table 2 shows the typical values of model parameters.

### 3.13. Computation procedure

Proposed model was developed by the following steps as described below.

**Table 3**
Values of kinetic parameters for growth model of *C. glutamicum* (NCIM-2168).

| Kinetic parameters | Unit | Values |
|---|---|---|
| Biomass production model | | |
| $K_{sl,X}$ | g/L | 0.75 |
| $K_{si}$ | g/L | 105.6 |
| $K_{glu,X}$ | g/L | 1.79 |
| $K_{fru,X}$ | g/L | 1.21 |
| $K_{pi,X}$ | g/L | 10.02 |
| Sugar utilization model | | |
| $q_{s,max}$ | g/g h | 2.35 |
| $K_{si,s}$ | g/L | 66 |
| $K_{sl,s}$ | g/L | 0.12 |
| $K_{si,GA}$ | g/L | 12 |
| Glutamic acid production model | | |
| $q_{GA,max}$ | g/g.h | 1.62 |
| $K_{si,GA}$ | g/L | 111 |
| $K_{sl,GA}$ | g/L | 1.12 |
| $K_{pi,GA}$ | g/L | 72 |

a Computation of GA ions concentration (Eq. (29)) at the membrane surface is the first step for the calculation of model predictive values of solute flux, volumetric flux and rejection.
b $\Delta c_{W,GA}$ and $c_{W,GA_{av}}$ were computed using Eqs. (31) and (32) and checking the guess value of $C_{p,F}$ using Eq. (33).
c The next step is to calculate permeate concentration of GA ions using Eq. (33).
d GA ions separation was then calculated using Eq. (34) where solute flux and volumetric flux were calculated using Eqs. (21) and (35) respectively.
e Membrane wall concentration of glutamate ion may be computed next by the help of Eq. (36) (concentration polarization modulus) with help of calculated rejection and solvent flux data and it was changed by different cross flow velocity and with the tim This changed value was then used as the membrane surface concentration of the respective solute for further calculation.

### 3.14. Analysis of error

By using standard statistical methods of calculation like root mean square, relative error (RE) and Willmott index ($d$), error analysis was done.

$$\mathrm{RE} = \frac{\sqrt{\Sigma_{i=1}^{n}(P_i - O_i)^2}/n}{\bar{O}} \tag{46}$$

where $O_i$ = experimental values, $\bar{O}$ = mean of experimentally observed result, $P_i$ = model predicted value and $n$ = number of sample points

$$d = 1 - \frac{\sum_{i=1}^{n}(P_i - O_i)^2}{\sum_{i=1}^{n}\left(|P_i - \bar{O}_i| + |O_i - \bar{O}|\right)^2} \tag{47}$$

## 4. Results and discussion

### 4.1. Biomass growth during GA fermentation

Fermentation was started with carbon source as sugarcane juice contained 11.0% (w/v) fermentable sugar (sucrose, 97.7 g/L; glucose 7.2 g/L and fructose 5.35 g/L) along with production medium (see section 3.2). It was observed during experimental investigation that glucose and fructose got consumed within initial 4–5 h of fermentation. The $K_{glu,X}$ and $K_{fru,X}$ values were estimated to be 1.79 g/L and 1.21 g/L respectively but these parameters did not exhibit any significant impact on the kinetics. Glucose and fructose had negligible effect on the specific growth rate of bacteria compared to that of sucrose due to low initial concentration of glucose and fructose. Table 3 shows the estimated values of kinetic parameters obtained by concentration profile of microbial growth. The substrate limitation constant ($K_{sl,X}$) for *C. glutamicum* growth was calculated 0.75 g/L. The $K_{si}$ value for the biomass growth was estimated 105.6 g/L and thus negligible inhibition would occur because the initial sugar concentration below $K_{si}$ value. The cell death coefficient ($K_d$) in Eq. (2) shows the decrease in biomass concentration at the end of the exponential phase as exhibited in Fig. 2. The value of $K_d$ depends upon the initial concentration of total sugar in the fermentation medium [27] and it has 0.02 $h^{-1}$ in present case.

### 4.2. Substrate consumption

After initial lag phase the substrate (sugar) concentration began to decrease along with gradual increase in product. The value of $K_{si,s}$ (substrate inhibition constant for sugar consumption) was calculated 66.4 g/L from the sugar consumption model. Such value of $K_{si,s}$ shows that substrate inhibition had insignificant impact on the sugar consumption by the microorganism as also reported by Hofvendahl and Hagerdal [33]. The carbon source (sugar) consumption was measured as maximum specific sugar uptake rate ($q_{s,max}$) which was estimated 1.62 g/(g h). During substrate consumption with time $K_{pi,s}$ and $K_{si,s}$ were estimated 12 g/L and 0.12 g/L, respectively. As shown in the Fig. 2 the model values of substrate consumption corroborated well with the experimental observation.

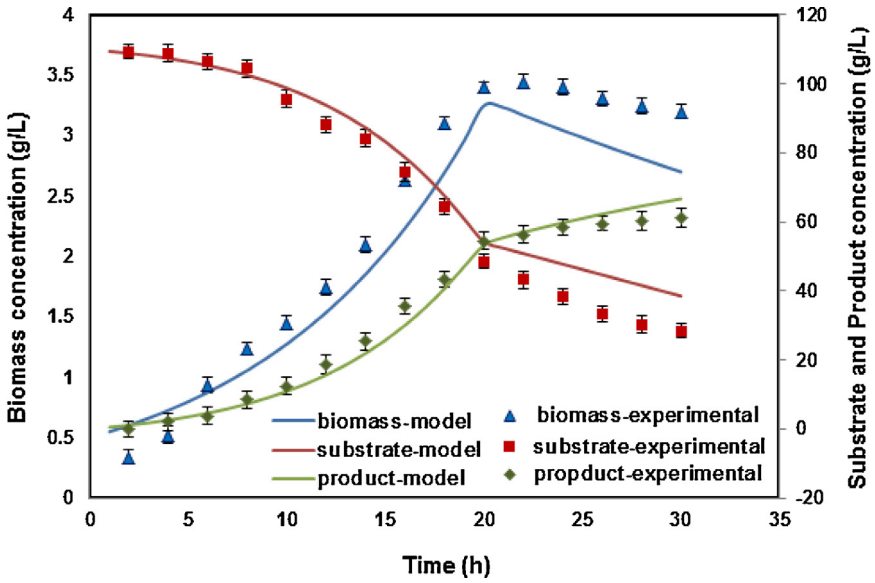


**Fig. 2.** Model predicted and experimentally obtained profile of growth of biomass concentration, glutamic acid production and sugar concentration at different time intervals.

### 4.3. Product formation during fermentation

During initial hours of the fermentation (8 h), the concentration of GA increased to a level of 25 g/L. Exponential growth phase of the *C. glutamicum* (NCIM-2168) continues till 20–24 h and growth associated product generated after that non-growth associated product formation occurs due to product inhibition. The substrate limitation constant $K_{sl,GA}$ and inhibition constant $K_{si,GA}$ for GA production were 1.12 g/L and 111 g/L, respectively as calculated from the model. During fermentation the pH of the broth drops 4.5 at the end of the fermentation under non-neutralizing conditions. Due to low p$K_a$ value of GA (2.10) and according to Henderson–Hasselbalch equation [34], at such pH of the fermentation broth. Maximum GA present in the broth is in an un-dissociated condition so product inhibition is only due to $K_{pi,GA}$ which is calculated to be 72 g/L. The estimated $q_{GA,max}$ value was nearly same 1.62 g/(gh) Fig. 2 shows the correlation of the model prediction with the experimental observations.

### 4.4. Simulation of the two stage membrane-integrated system during continuous fermentation

During continuous fermentation membrane-integrated system permeate flow rate from the MF module were maintained same with the addition of fresh feed (i.e., dilution rates) by adjusting the by-pass valves in the flow line and also with the permeate flow rates from the NF module. During continuous production of GA in the membrane-integrated system lag phase of the growth of the micro-organism (*C. glutamicum* NCIM-2168) was barely seen because of use of well-established and pre-inoculated and nutrient-supplemented inoculum. The microbes are in strongly active dividing stage in the exponential phase after 20 h of initial fermentation time. The introduction of fresh feed as well as recycling of the cells during continuous fermentation, the product formation kinetics changed. The effect of different dilution rates (0.1 $h^{-1}$, 0.14 $h^{-1}$ and 0.18 $h^{-1}$) on experimental and model predicted biomass concentration profiles were shown in the Fig. 3 (a). The volumetric flow rate inputs to microfiltration units were maintained 150 L/($m^2$h) (0.5 m/s), 250 L/($m^2$h) (0.9 m/s) and 350 L/($m^2$h)(1.2 m/s) with respective dilution rates. It is quite obvious that microbial concentration profiles in all the experiments declined just after the starting of microfiltration till steady state was not achieved. The concentration of microbial cell concentration decreased as the cross-flow velocity as well as fresh feed dilutions were increased. The experimentally found value of $\mu_{net}$ was incorporated in the model to describe the initial growth pattern of the *C. glutamicum* (NCIM-2168) just after the start of continuous fermentation. At higher cross-flow velocity during microfiltration, specific growth rate, product formation and substrate consumption profile suffered due to fluctuation in microbial cell concentration. By proper cell bleeding such fluctuation periods were smoothed out and $\mu_{net}$ values was kept constant on 0.2, 0.35 and 0.45 with respective cross-flow velocity of 0.53 m/s, 0.88 m/s and 1.23 m/s to achieve the steady state condition.

The maximum specific GA production and sucrose utilization rates were changed to 1.62 g/gh and 2.35 g/gh, respectively with the introduction of fresh feed into the system. The dilution rate was varied to 0.1 $h^{-1}$, 0.14 $h^{-1}$ and 0.18 $h^{-1}$. At the initial hours of continuous fermentation, the strain present in the fermentation broth takes some lag phase which results into slowdown of specific rate of sucrose consumption and GA production. It is quite obvious that increase in the dilution rates the rate of sucrose consumption decreases. The Fig. 2(b) and (c) shows the model predicted versus the experimental breakthrough curves for sucrose utilization and GA production respectively at various dilution rates during continuous production. It was assumed that the nutrient present in the $F_{nf,rec}$ negligible so, the $F_{nf,i}$ and $F_{nf,out}$ were contributed significantly on the production of GA. By adjusting the cell bleeding the specific growth rate was smoothed out and similarly the fluctuation in sucrose utilization and GA production come to streamline at steady state. At dilution rate 0.1 $h^{-1}$, 0.14 $h^{-1}$, 0.18 $h^{-1}$ the yield were achieved 85%, 86%, 87% with respective productivities 6.6 g/L/h, 8.5 g/L/h and 9.3 g/L/h. The product concentration at these different dilution rate during steady state conditions, were 66 g/L, 61 g/L and 54 g/L and respective cross-flow velocities 0.5 m/s, 0.9 m/s and 1.3 m/s. Similar types of result of sugar consumption profile by incorporating dilution rates (D) directly in the model equation has been found [35]. For the continuous operation the lowest dilution rate 0.1 $h^{-1}$ was selected due to highest sucrose to GA conversion rate was achieved.

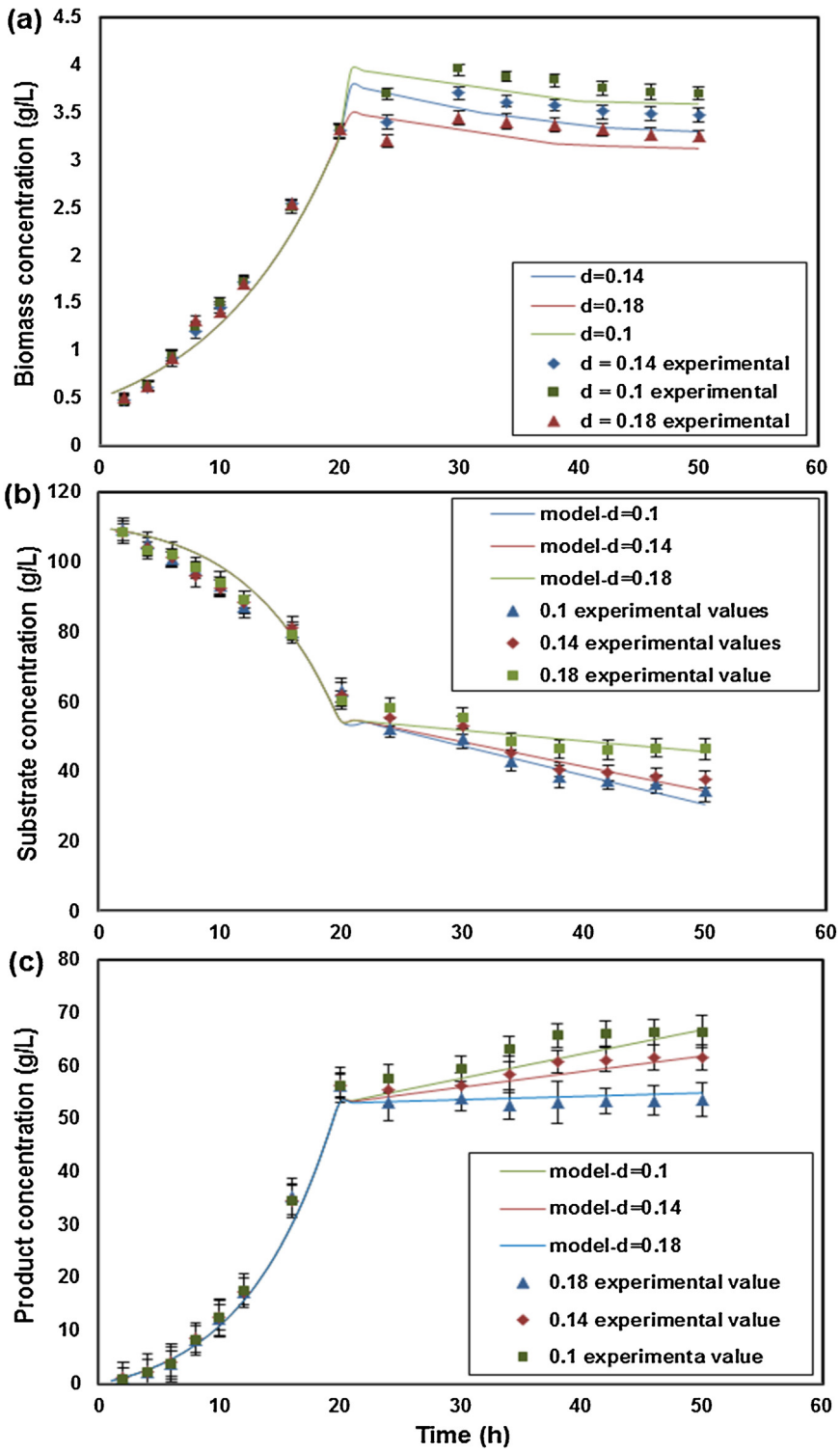


**Fig. 3.** Experimentally verified model values during continuous fermentation of glutamic acid at different fresh feed dilution rate influenced by different cross-flow velocity inside the fermenter, (a) biomass concentration profiles; (b) sugar consumption rates; (c) glutamic acid production profile.

### *4.5. Flux during nanofiltration under varying operating pressure: model Vs experimental values*

Microfiltered fermentation broth containing 55 g/L GA was made to pass through the nanofiltration module. In Fig. 4 shows the flux behaviour of nanofiltration membranes (NF-1, NF-2, NF-3 and NF-20) under varying operating pressures. The transmembrane pressure was varied from 0 to 15 bars for all four membranes. The flux was varied linearly with applied pressure. The highest flux 220 L/($m^2$h) was shown by NF-2 membrane whereas NF-1 shows the minimum 70 L/($m^2$h) at an operating transmembrane pressure of 15 bar and cross-flow velocity 3.4 m/s. The model predicted values were found to be well in agreement with the experimental observations.

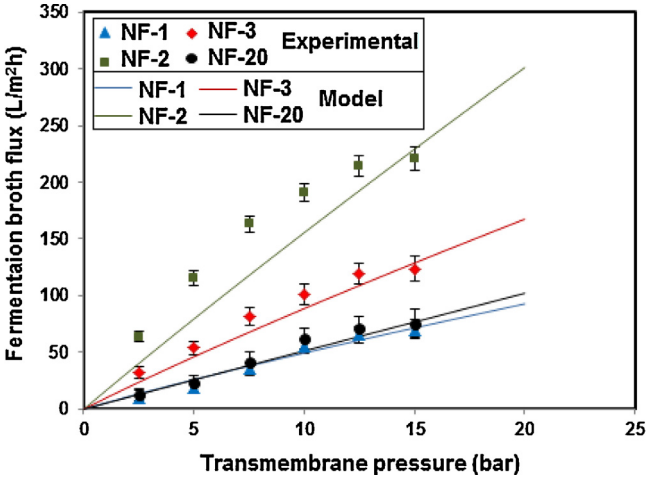


**Fig. 4.** Model predicted and experimentally obtained profile on microfiltered fermentation broth flux at different transmembrane pressure during nanofiltration by four different types of NF membranes.

Flux was affected due to fouling of membrane and membrane resistance which is internal properties of the membrane. In addition to membrane resistance, membrane fouling resistance and cake layer resistance on the surface of the membrane are responsible for the change in the permeate flux. Reduction of fouling and formation of cake on the membrane surface was made possible due to cross flow mode of membrane modules which was generated high sweeping action over the membrane surface. However, due to solution hydrodynamics, the cake layer and fouling resistance increases during long term of operation with time. The drop in flux does not warrant replacement of the membrane. The cleaning of fouled membrane after filtration experiment may be done using deionized water, 0.01 M NaOH (pH 11) and NaOCl (200 mg/L) to recover the flux performance. The product purification was done by second stage of membrane filtration by employing NF-20 membrane in cross-flow membrane module. A permeate flux 75 L/($m^2$h) was achieved by maintaining cross-flow velocity at 3.4 m/s and transmembrane pressure was maintained 15 bar.

### 4.6. Downstream glutamic acid purification through nanofiltration

Rejection or permeation behaviour of GA and sucrose may be explained Donnan exclusion principle which applied on nanofiltration membranes. Fig. 5(a) and (b) shows the model and experimental values of rejection characteristic of GA and sucrose by four different membranes. NF-20 membrane ensured high rejection of unconverted carbon source i.e., sucrose (95%) due to steric effect of the membrane and permeated more than 85% GA ions because of low concentration electrically charged group present on the membrane surface. Thus, unconverted carbon source and ions like $Mg^{2+}$, $Ca^{2+}$, $K^+$ and $Na^+$ were recycle back to the fermenter which make the process economical. High negative surface charge density and low pore size of NF-1 membrane makes in high rejection of GA and sucrose in comparison to other membranes. The transmembrane pressure beyond 15 bar hardly lead to further increase in rejection of undesirable solutes though flux continued to increase as obvious in pressure driven filtration system. Size exclusion, solution diffusion and Donnan exclusion are the mechanism responsible for the separation GA, sucrose and other components. In solution-diffusion mechanism the solute flux and solvent fluxes remain uncoupled; hence increase in transmembrane pressure increases solvent flux without affecting solute rejection. Charged based separating mechanism may be explained by Donnan exclusion mechanism. Model and experimental values were found to be in good agreement to each other.

### 4.7. Cross flow rate: effect on flux and rejection

The cross flow velocity of microfiltered fermentation broth was varied from 200 L/h to 700 L/h over the surface of the nanofiltration membrane while keeping the transmembrane pressure fixed at 15 bar. It was found that at higher cross flow velocity the flux was high for all four different types of nanofiltration membranes. The highest flux 220 L/($m^2$h) at cross flow velocity 1.25 m/s was produced by NF-2 membrane whereas the lowest flux 70 L/($m^2$h) was yielded by NF-1 membrane under same operating conditions. This is due to NF-1 membrane was tightest in nature whereas NF-2 was loosest one among all four NF membranes. However, the highest rejection was achieved in case of NF-1 membrane due to high concentration of electrically charged group on its surface whereas lowest was found in case of NF-20 membrane. The Fig. 6(a) and (b) shows the flux and rejection trend by four different types of NF membranes with varying cross flow velocities which clearly show that increase in cross flow velocity increases flux as well as rejection in all cases. The rejection of GA increases from 82% to 97.5%; 28% to 42%; 71% to 83% and 11% to 15% in case of NF-1, NF-2, NF-3 and NF-20 as the cross flow velocity was increased from 200 L/h to 700 L/h. As the sweeping action is enhanced by increasing the cross flow velocity due to solvent flux in case of nanofiltration membrane, resulting higher retention of GA due to uncoupling nature of solute and solvent fluxes. The effect of concentration polarization was also reduced due to cross flow velocity of feed by producing high sweeping action over the surface of the membrane. Thus effect of fouling could also be significantly reduced at higher cross flow velocity.

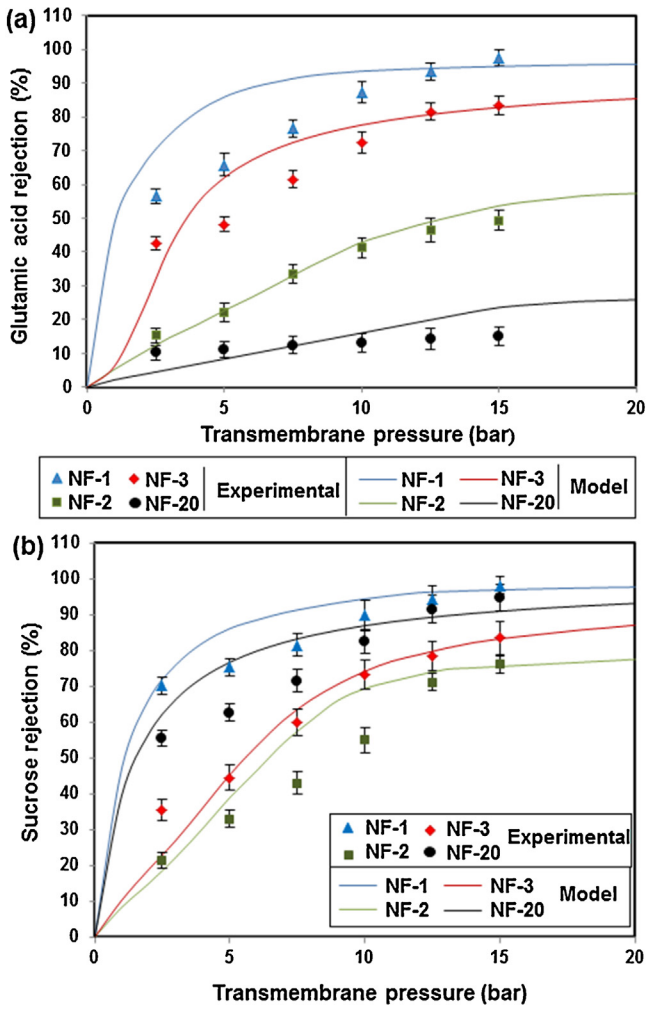


**Fig. 5.** Model predicted and experimentally obtained profile on rejection of (a) glutamic acid; (b) sucrose at different transmembrane pressure during nanofiltration by four different types of NF membranes.

**Table 4**
Error analyses for model fitness using biomass concentration, substrate concentration, product concentration, fermentation broth flux and GA rejection data.

| Figures | Investigation nature | Errors data | | |
|---|---|---|---|---|
| | | RE | $R^2$ | $d_{\text{will-index}}$ |
| Fig. 2 | Biomass conc. vs time (batch) | 0.09 | 0.98 | 0.96 |
| Fig. 2 | Substrate conc. vs time (batch) | 0.10 | 0.98 | 0.96 |
| Fig. 2 | Product conc. vs time (batch) | 0.08 | 0.99 | 0.97 |
| Fig. 3a | Biomass conc. vs time (continuous) | 0.09 | 0.98 | 0.96 |
| Fig. 3b | Substrate conc. vs time (continuous) | 0.11 | 0.97 | 0.95 |
| Fig. 3c | Product conc. vs time (continuous) | 0.08 | 0.99 | 0.97 |
| Fig. 4 | Broth flux vs pressure (NF-1) | 0.08 | 0.99 | 0.98 |
| Fig. 5a | GA rejection vs pressure (NF-1) | 0.10 | 0.98 | 0.95 |
| Fig. 5b | Broth flux vs cross flow rate (NF-1) | 0.08 | 0.99 | 0.98 |
| Fig. 6b | GA rejection vs cross flow rate (NF-1) | 0.09 | 0.99 | 0.98 |

### *4.8. Model performance by error analysis*

Model validation in terms of relative errors, regression coefficient and Willmott-d-index indicates that developed model is reasonably successful. Table 4 shows that relative error is low (<0.05) whereas overall correlation coefficient ($R^2 > 0.98$) and Willmott-*d*-index ($d > 0.97$) are quite high reflecting good performance of the model.

## 5. Economic evaluation of the membrane-integrated, fermentative production scheme

The membrane integrated production scheme offers economic advantages over the conventional schemes on quite a few counts like cost of raw material and cost of downstream purification. Use of sugarcane juice as a cheap, easily available and renewal raw material drastically cuts down cost of fermentative production where the pre-treatment steps such as liquefaction and saccharification are not

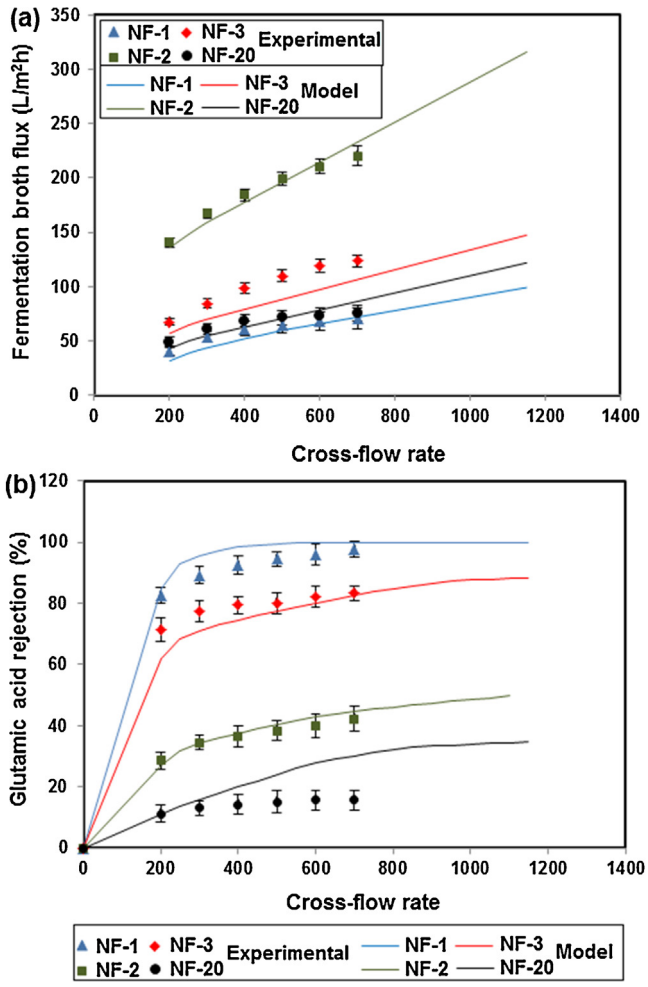


**Fig. 6.** Effect of cross-flow rate on (a) flux of microfiltered fermentation broth; (b) rejection of glutamic acid, model predicted values with experimental one.

redundant. Moreover, the proposed carbon source (sugarcane) is available at a relatively low price almost throughout the year in major sugar cane growing big countries like India and Brazil. In India, sugarcane growers will be protected from distress sale of their produce. An economic analysis for industrial production of 1550 t per annum of GA was done in this study to examine economic competitiveness of the proposed new process assuming 300 working days in a year with production in 3 shifts (each of 8 h). Capital costs on civil investment, storage tank, fermenter, pumps, membrane modules, stainless steel pipelines, power consumption, depreciation and insurances and the operational cost involving raw materials, labours, membranes, maintenance and utility were computed. This new design reflected high process intensification that can be operated with 35–40 persons at any instant of time. The pilot plant was scaled-up up to a level of 1550 t per year based on the standard scale up principles [36] as below.

$$\text{Cost ofhighercapacity equipment} = \text{Cost of labscaleequipment} \times \left[\frac{\text{capacityofhighcapacityequipment}}{\text{capacityoflabscaleequipment}}\right]^{n}$$

where, $n$ represents the scale-up factor and differs for different equipment, $n$ values were taken from the list mentioned by Ulrich [37].

The power consumption for agitators was calculated using following equation:

$$P = N_p \rho N^3 D_a^5$$

where $P$ represents power in $W$, $N_p$ represents power number, $\rho$ is fluid density, $N$ is rotational speed in rev/s and $D_a$ is impeller diameter in $m$. The agitator was assumed to be flat six-blade turbine and scale up by following equation:

$$N_2 = N_1 \left(\frac{1}{R}\right)^{n}$$

where $R$ represents scale-up ratio, $N_1$ and $N_2$ are agitator speed for reference and lab scale unit respectively and $n$ is empirical constant. An exchange rate of 62.0 INR/US$ was considered for the conversion of Indian cost data to US$. A payback period of 15 years and an interest rate of 9% have been assumed.

GA production = 1550 ton/year = 5160 kg/day = 215 kg/h

1 $m^2$ membrane surface area is producing flux 75 L/h with 55 g/L GA concentration.

Each 0.15 $m^2$ membrane module surface area is producing GA = 0.15 × 75 × 55 × 24 = 14.6 kg/day

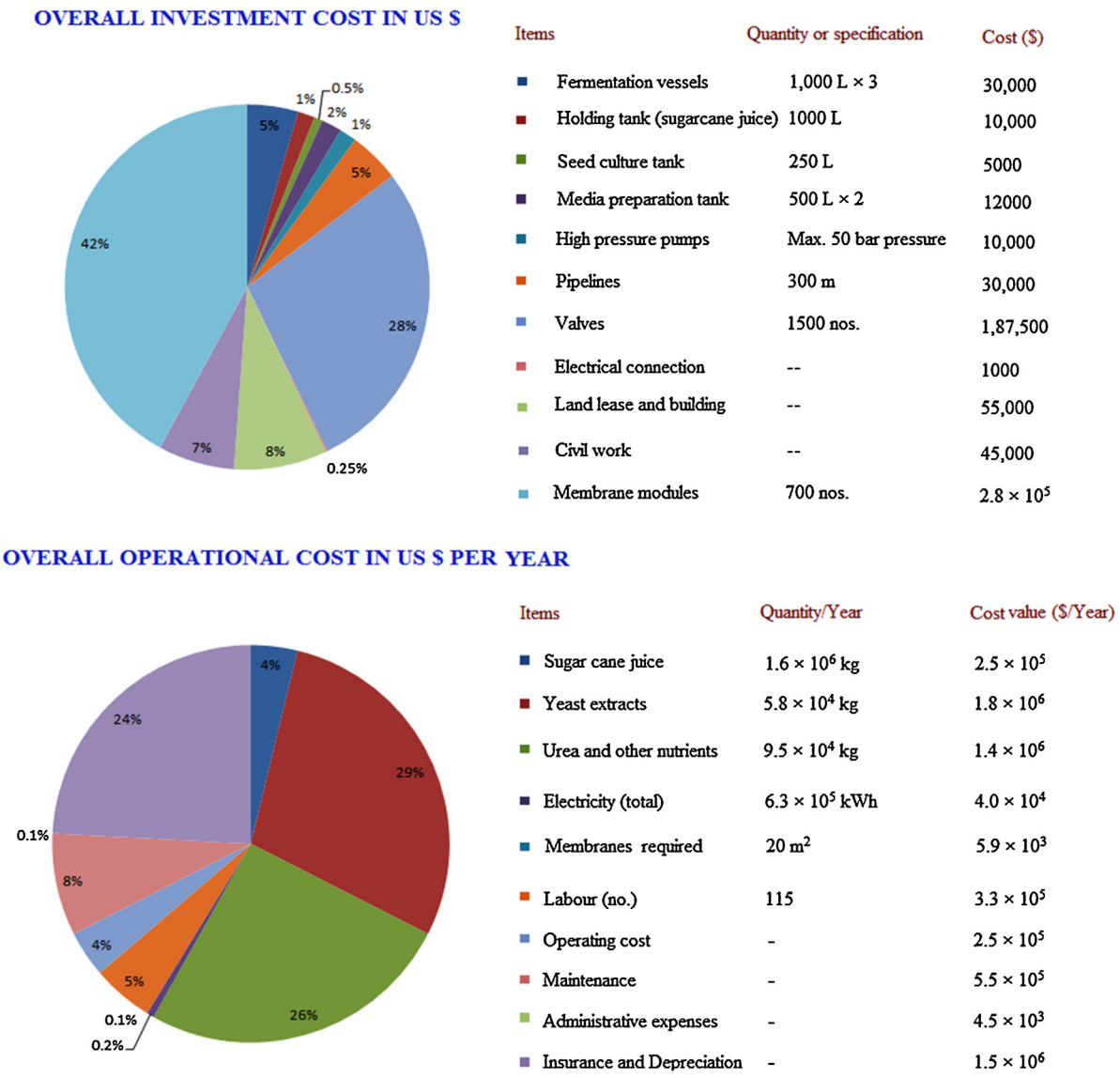


**Fig. 7.** Capital iinvestment and operational cost involved for the production of glutamic acid of plant capacity: 1550 tonnes/year.

Number of membrane modules required in each filtration section ($n$)

$$n = \frac{\text{required output per day(kg)}}{\text{Output per module per day(kg)}}$$

So, total ~700 membrane modules are required for MF and NF.

The annualized capital cost was calculated as:

$$\frac{(\text{Total capital cost} \times \text{Capital recovery factor})}{\text{Annual output rate(kg per year)}}$$

$$\text{Capital recovery factor} = \left[\frac{i(1+i)^n}{(1+i)^{n+1}-1}\right] = 0.087$$

'$n$' and '$i$' were considered to be is the project life of the plant and the rate of interest as per market statistics.

So, the annualized capital cost is evaluated as:

$$\left[\frac{661250 \times 0.087}{1550000}\right] = 0.04$$

The annualized operating cost ($/kg) was evaluated as:

$$= \frac{\text{Total annual cost(?)}}{\text{Output per year(kg)}} = \left[\frac{6600000}{1550000}\right] = 4.26$$

The estimated cost of capital items and recurring items comprises different components as have been shown in Fig. 7. More than 60% of the annual operating cost is on the nutrient. As a standard practice, 24% of the fixed capital investment has been considered on insurance and depreciation cost. Total annualized production cost is evaluated by adding annualized capital cost and annualized operational cost which is found to be (0.04 + 4.26) = 4.3 $/kg of GA and is considerably lower than the existing market selling price of similar grade of GA

(US $ ~ 9/kg for same purity). These selling prices ($ 9–10/kg) are observed on the websites of some glutamic acid manufacturers such as Shaanxi Fuheng (FH) Biotechnology Co., Ltd.; Located in Hi-Tech Industrial District of Xi'an, Xi'an Lyphar Biotech Co., Ltd.; Xi'an City, Shannxi Province, China, Xi'an Miracle Biotechnology Co., Ltd.; Shaanxi, China.

An economic advantage for production of GA through new membrane-integrated scheme is thus obvious though the reflected cost here should be considered as preliminary estimate based on Indian market conditions. Despite the possibility of marginal variation of cost in different conditions, savings on manpower, energy, raw materials, equipment are quite obvious in the new process due to its high degree of process intensification. Modular design also provides scope for change in capacity utilization without affecting economy. Thus, the process and the design that developed from this research are blessed with the environmental benefits such as the minimum generation of waste, absence of harsh chemicals in the process, consumption of low energy compared to that required in a multi-step conventional process.

Economic analysis that has been presented here based on laboratory scale study is only to give an idea about the economic viability of the proposed process. Though a much simplified production scheme, significantly reduced unit operations and possibility of involvement of reduced capital, use of low cost renewable raw material as carbon source, possibility of continuous and direct production of GA with high purity (by high selectivity of tailor-made membranes) and higher productivity vis-à-vis traditional processes are enough indications of the economic viability of the proposed process, we attempted to present a simple, preliminary economic analysis to show that the new process has potential of production with reasonable profit margin in a green process where the product is also expected to be of better quality.

The price of $ 4.3/kg of glutamic acid has been arrived here considering the major cost factors as mentioned in the economic analysis section. This price should be taken as an indicative price only and not as actual retail price.

## 6. Conclusion

The continuous fermentative production of glutamic acid in a membrane-integrated hybrid reactor system has been modeled considering microbial kinetics under substrate-product inhibitions and the transport phenomena during downstream separation through nanofiltration membrane. The performance of the fully membrane-integrated hybrid process for direct production of glutamic acid could be successfully predicted as evident in high average correlation coefficient value ($R^2 > 0.98$) and high Willmott *d*-index value (>0.98). The developed model coupled with preliminary economic evaluation for a green, fermentative process for production of glutamic acid from a renewable carbon source in a continuous, simple, compact and eco-friendly production plant is expected to facilitate industrial scale up.

## Acknowledgements

Authors are thankful to the Department of Science and Technology, Government of India for financial support under Start-Up Research Grant for Young Scientist (Science and Engineering Research Board) [SB/FTB/ETA-059/2013].

## References

[1] K. Drauz, I. Grayson, A. Kleemann, H.-P. Krimmer, W. Leuchtenberger, C. Weckbecker, Amino Acids, Ullman's Encyclopaedia of Industrial Chemistry, 7th Ed., Wiley, 2007.
[2] R. Kumar, D. Vikramachakravarthi, P. Pal, Production and purification of glutamic acid: a critical review towards process intensification, Chem. Eng. Process. Process Intensif. 81 (2014) 59–71.
[3] D. Vikrama Chakravarthi, R. Kumar, P. Pal, Direct production of L (+) glutamic acid in a continuous and fully membrane-integrated hybrid reactor system under non-neutralizing conditions, Ind. Eng. Chem. Res. 53 (2014) 19019–19027.
[4] S. Kinoshita, S. Udaka, M. Shimono, Amino acid fermentation. I. Production of L-gLutamic acid by various micro-organism, J. Gen. Appl. Microbiol. 3 (1957) 177–199.
[5] K.M. Nampoothiri, A. Pandey, Immobilization of Brevibacterium cells for the production of L-glutamic acid, Bioresour. Technol. 63 (1998) 101–106.
[6] I. Sunitha, M.V.S. Rao, C. Ayyanna, Optimization of medium constituents and fermentation conditions for the production of L-gLutamic acid by the co-immobilized whole cells of *Micrococcus glutamicus* and *Pseudomonas reptilivora*, Bioprocess. Eng. 18 (1998) 353–359.
[7] R. Kumar, P. Pal, Fermentative production of poly (γ-glutamic acid) from renewable carbon source and downstream purification through a continuous membrane-integrated hybrid process, Bioresour. Technol. 177 (2015) 141–148.
[8] N.S. Khan, I.M. Mishra, R.P. Singh, B. Prasad, Modeling the growth of *Corynebacterium glutamicum* under product inhibition in L-glutamic acid fermentation, Biochem. Eng. J. 25 (2005) 173–178.
[9] R. Bona, A. Moser, Modeling of the L-glutamic acid production with *Corynebacterium glutamicum* under biotin limitation, Bioprocess Eng. 17 (1997) 139–142.
[10] A. Moser, Bioprocess Technology, Kinetics and Reactors, Springer-Verlag, New York, Wien, 1988.
[11] X.-W. Zhang, T. Sun, Z.-Y. Sun, X. Liu, D.-X. Gu, Time-dependent kinetic models for glutamic acid fermentation, Enzyme Microb. Technol. 22 (1998) 205–209.
[12] O. Levenspiel, The Monod equation: a revisit and a generalization to product inhibition situations, Biotechnol. Bioeng. 22 (1980) 1671–1687.
[13] N.A. Mostafa, Production of acetic acid and glycerol from salted and dried whey in a membrane cell recycle bioreactor, Energy Convers. Manage. 42 (2001) 1133–1142.
[14] D.L. Grzenia, D.J. Schell, S.R. Wickramasinghe, Membrane extraction for removal of acetic acid from biomass hydrolysates, J. Membr. Sci. 322 (2008) 189–195.
[15] P. Pal, J. Sikder, S. Roy, L. Giorno, Process intensification in lactic acid production: a review of membrane based processes, Chem. Eng. Process. 48 (2009) 1549–1559.
[16] Z. Kovács, M. Discacciati, W. Samhaber, Modeling of amino acid nanofiltration by irreversible thermodynamics, J. Membr. Sci. 332 (2009) 38–49.
[17] Z. Kovács, W. Samhaber, Nanofiltration of concentrated amino acid solutions, Desalination 240 (2009) 78–88.
[18] T. Gotoh, H. Iguci, K. Kikuchi, Separation of glutathione and its related amino acids by nanofiltration, Biochem. Eng. J. 19 (2004) 165–170.
[19] T. Tsuru, T. Shutou, S. Nakao, S. Kimura, Peptide and amino acid separation with nanofiltration membranes, Sep. Sci. Technol. 29 (8) (1994) 971–984.
[20] H.N. Chang, N. Kim, J. Kang, C.M. Jeong, J. Choi, Q. Fei, B.J. Kim, S. Kwon, S.Y. Lee, J. Kim, Multi-stage high cell continuous fermentation for high productivity and titer, Bioprocess Biosyst. Eng. 34 (2011) 419–431.
[21] A.A. Hussain, M.E.E. Abashar, I.S. Al-Mutaz, Effect of Ion sizes on separation characteristics of nanofiltration membrane systems, J. King Saudi Univ. Eng. Sci. 19 (2006) 1–19.
[22] W.R. Bowen, J.S. Welfoot, Modeling the performance of membrane nanofiltration: critical assessment and model development, Chem. Eng. Sci. 57 (2002) 1121–1137.
[23] D. Bhattacharyya, M.E. Williams, Reverse osmosis, in: W.S. Ho, K.K. Sirkar (Eds.), Membrane Handbook, Springer Science, Van Nostrandi Reinhold, New York, USA, 1992, pp. 263–390.
[24] D. Nancib, Lactic Acid Production by *Lactobacillus Casei* Subsp. Rhamnosus Growing on Date Juice: Batch, Fed-batch and Continuous Culture Kinetics and Optimization, University of Nancy, Nancy, France, 2007 (thesis).
[25] A.D. Nandasana, S. Kumar, Kinetic modelling of lactic acid production from molasses using *Enterococcus faecalis* RKY1, Biochem. Eng. J. 38 (2008) 277–284.
[26] A. Nishiwaki, Analysis of a two-stage fermenter with cell recycling for continuous acetic acid production, J. Biosci. Bioeng. 83 (1997) 565–570.
[27] P. Dey, P. Pal, Modelling and simulation of continuous L (+) lactic acid production from sugarcane juice in membrane integrated hybrid-reactor system, Biochem. Eng. J. 79 (2013) 15–24.
[28] F.Y. Yamashita, T. Kokugan, An improved model for cross-flow microfiltration properties of lactic acid fermentation broth, J. Chem. Eng. Jpn. 43 (2010) 993–997.

[29] J. Nayak, M. Pal, P. Pal, Modeling and simulation of direct production of acetic acid from cheese whey in a multi-stage membrane-integrated bioreactor, Biochem. Eng. J. 93 (2015) 179–195.
[30] A. Szymczyk, P. Fievet, Ion transport through nanofiltration membranes: the steric, electric and dielectric exclusion model, Desalination 200 (2006) 122–124.
[31] Y. Hirose, H. Enei, H. Shibai, l-Glutamic acid fermentation, in: M. Moo-Young (Ed.), Comprehensive Biotechnology, first ed., Pergamon Press, New York, 1985, pp. 593–600.
[32] S.-U. Choi, T. Nihira, T. Yoshida, Enhanced glutamic acid production of *Brevibacterium* sp. with temperature shift-up cultivation, J. Biosci. Bioeng. 98 (3) (2004) 211–213.
[33] K. Hofvendahl, B.H. Hagerdal, Factors affecting the fermentative lactic acid production from renewable resources, Enzyme Microb. Technol. 26 (2000) 87–107.
[34] M.I. Gonzalez, S. Alvarez, F.A. Riera, R. Alvarez, Lactic acid recovery from whey ultra-filtrate fermentation broths and artificial solutions by nanofiltration, Desalination 228 (2008) 84–96.
[35] A. Nishiwaki, I.J. Dunn, Performance of a two-stage fermenter with cell recycle for continuous production of lactic acid, Bioprocess Eng. 21 (1999) 299–305.
[36] Plant Design and Economics for Chemical Engineers, in: M.S. Peters, K.D. Timmerhaus, R.E. West (Eds.), McGraw-Hill, New York, 2003, pp. 163–170.
[37] G.D. Ulrich, A Guide to Chemical Engineering Process Design and Economics, John Wiley & Sons, USA, 1984, 267 pp.